Photorealistic Models for Pupil Light Reflex and Iridal Pattern Deformation

VITOR F. PAMPLONA and MANUEL M. OLIVEIRA
Universidade Federal do Rio Grande do Sul
and
GLADIMIR V. G. BARANOSKI
University of Waterloo

We introduce a physiologically-based model for pupil light reflex (PLR) and an image-based model for iridal pattern deformation. Our PLR model expresses the pupil diameter as a function of the lighting of the environment, and is described by a delay-differential equation, naturally adapting the pupil diameter even to abrupt changes in light conditions. Since the parameters of our PLR model were derived from measured data, it correctly simulates the actual behavior of the human pupil. Another contribution of our work is a model for realistic deformation of the iris pattern as a function of pupil dilation and constriction. Our models produce high-fidelity appearance effects and can be used to produce real-time predictive animations of the pupil and iris under variable lighting conditions. We assess the predictability and quality of our simulations through comparisons of modeled results against measured data derived from experiments also described in this work. Combined, our models can bring facial animation to new photorealistic standards.

Categories and Subject Descriptors: I.3.7 [**Computer Graphics**]: Three-Dimensional Graphics and Realism—*Animation*; I.3.5 [**Computer Graphics**]: Computational Geometry and Object Modeling—*Physically based modeling*

General Terms: Experimentation, Human Factors

Additional Key Words and Phrases: Face animation, image-based modelling, iris animation, photorealism, physiologically-based modelling

ACM Reference Format:

Pamplona, V. F., Oliveira, M. M., and Baranoski, G. V. G. 2009. Photorealistic models for pupil light reflex and iridal pattern deformation. ACM Trans. Graph. 28, 4, Article 106 (August 2009), 12 pages. DOI = 10.1145/1559755.1559763 http://doi.acm.org/10.1145/1559755.1559763

1. INTRODUCTION

Arguably, the most important features in facial animation are the eyes, which are essential not only in directing the gaze of the audience [Lee et al. 2002], but also in conveying the appropriate degree of expression through pupil dilation and constriction movements [Watt and Watt 1992]. Hence, for animations depicting close-up views of the face, natural-looking eyes and pupil movements are highly desirable.

> "Walt Disney once said to his animation team that the audience watches the eyes and this is where the time and money must be spent if the character is to act convincingly" [Watt and Watt 1992].

Differently from most of the body, the human eye is subject to some involuntary movements of the pupil, which are determined by ambient illumination, drug action, and emotional conditions, among others [Reeves 1920; Calcagnini et al. 2000]. Pupillary light reflex (PLR) is responsible for the constriction of the pupil area in highly lit environments and for its dilation in dimmed ones. PLR is an integral part of our daily experience, and except for drug-induced action, is the single most noticeable of such involuntary movements of the pupil.

The human iris is a muscular tissue containing several easily identifiable structures. Together, they define patterns that are deformed as a result of changes in the pupil diameter. Although pupil light reflex and iridal deformations could be animated using standard computer graphics techniques, such as parametric representations controlled by velocity curves, we believe that the use of physiologically-based models guided by physically meaningful parameters can make the process more predictable and automatic, which in turn, may result in more realistic and reproducible animations of these movements.

In this article, we present a physiologically-based model for realistic animation of PLR. Our model combines and extends some theoretical results from the field of mathematical biology [Longtin and Milton 1989] with experimental data collected by several

Manuel M. Oliveira acknowledges a CNPq-Brazil fellowship (305613/2007-3). Gladimir V. G. Baranoski acknowledges a NSERC-Canada grant (238337). Microsoft Brazil provided additional support.

Authors' addresses: V. F. Pamplona, email: vitor@vitorpamplona.com; M. M. Oliveira, email: oliveira@inf.ufrgs.br; G. V. G. Baranoski, email: gvgbaran@curumin.math.uwaterloo.ca

DOI 10.1145/1559755.1559763 http://doi.acm.org/10.1145/1559755.1559763

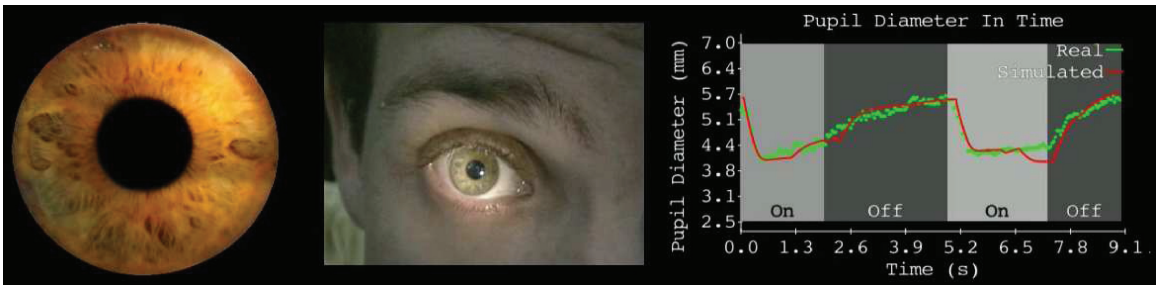

Fig. 1. Comparison of the results predicted by our models against video of a human iris. (left) One frame of an animation simulating the changes in pupil diameter and iridal pattern deformation. (center) One frame from a video of a human iris. (right) Graph comparing the measured pupil diameters from each individual frame of a nine-second-long video sequence (green line) against the behavior predicted by our model (red line). The gray bars indicate the periods in which the light was kept on and off. The complete video sequence and corresponding animation are shown in the accompanying video.

Table I. Summary of the Main Mathematical and Physical Quantities Considered in the Development of the Proposed Models

Symbol	Description	Physical Unit
L_b	luminance	blondels (B)
L_{fL}	luminance	foot-Lambert (fL)
I_l	illuminance	lumens/mm^2 (lm/mm^2)
R	light frequency	Hertz (Hz)
ϕ	retinal light flux	lumens (lm)
$\bar{\phi}$	retinal light flux threshold	lumens (lm)
D	pupil diameter	millimeters (mm)
A	pupil area	square millimeters (mm^2)
r_I	individual variability index	$r_I \in [0,1]$
t	current simulation time	milliseconds (ms)
τ	pupil latency	milliseconds (ms)
x	muscular activity	none
ρ_i	ratio describing the relative position of a point in the iridal disk	none
β, α, γ, k	constants of proportionality	none

researchers relating pupil diameter to the intensity of environmental light [Moon and Spencer 1944]. The resulting model produces high-fidelity appearance effects and can be used to produce real-time predictive animations of the pupil and iris under variable lighting conditions (Section 5.4). We model the iridal pattern deformation process by acquiring a set of high-resolution photographs of real irises at different levels of pupillary dilation and by tracking their features across the set of images. By analyzing the tracked positions, we obtained a simple analytical expression for the iridal deformation pattern as a function of the pupil diameter (Section 6). To the best our knowledge, ours is the first physiologically-based model for simulating pupil light reflex presented in the graphics literature (the first model ever to simulate individual variability in terms of PLR sensitivity—Section 5.3), as well as the first model for iridal pattern deformation. Moreover, ours are the first practical models (providing actual coefficient values) in the literature for simulating the dynamics of the pupil and iris under variable lighting conditions. We demonstrate the effectiveness of our approach by comparing the results predicted by our models against photographs and videos captured from real human irises (Figures 1 and 12). Table I summarizes the main mathematical and physical quantities used in the derivation of the proposed models and which are considered throughout this work.

2. RELATED WORK IN COMPUTER GRAPHICS

A few researchers have addressed the issue of realistic human iris synthesis. Lefohn et al. [2003] blend several textures created by an artist, each containing some eye feature. Other image-based approaches have been proposed by Cui et al. [2004], Wecker et al. [2005], and Makthal and Ross [2005]. Essentially, they decompose a set of iris images using techniques such as principal component analysis, multiresolution and wavelets, and Markov random fields, and recombine the obtained data to generate new images of irises. Zuo and Schmid [2005] created a fiber-based 3D model of the iris. Lam and Baranoski [2006] introduced a predictive light transport model for the human iris, which computes the spectral responses of iridal tissues described by biophysical parameters. François et al. [2007] estimate iris height maps from gray-scale images. All these approaches use stationary pupil sizes.

Sagar et al. [1994] developed an anatomically detailed model of the eye to be used in a surgical simulator. In their model, Gaussian perturbations were used to simulate the waviness of ciliary fibers and the retraction of pupillary fibers during pupil dilation. Alternatively, depending on the level of object manipulation, a texture mapping approach was used to model the iridal appearance. It is worth noting, however, that their goal was to achieve functional realism [Ferwerda 2003] as opposed to physical or photorealism.

3. BRIEF OVERVIEW OF THE HUMAN IRIS AND PUPIL

The human iris has a diameter of about 12 mm and forms a disc that controls how much light reaches the retina [Trevor-Roper and Curran 1984]. Under high levels of lighting, the iris dilates, flattening

itself and decreasing the pupil size. Under low levels of illumination, it constricts, folding itself and increasing the pupil area. The pupil diameter varies from 1.5 mm to 8 mm on average [Reeves 1920], and in general, it is not a perfect circle. Also, its center may deviate from the center of the iris by an offset of up to 20% [Trevor-Roper and Curran 1984]. According to Newsome and Loewenfeld [1971], there are no observable differences in the iris regarding light-induced or drug-induced pupil dilation/constriction.

The human iris is divided in two zones by the *collarette*, a delicate zig-zag line also known as the iris frill. The *pupillary* zone is bounded by the pupil, while the *ciliary* zone extends to the outer border of the iris. Each zone is characterized by a muscle. The *sphincter*, located in the pupillary zone, is a concentric muscle that constricts to decrease the pupil size. The *dilator*, found in the ciliary zone, is a radial muscle that constricts to increase the pupil size. These two muscles overlap at the collarette.

The sphincter and dilator muscles are independently connected to the autonomous nervous system (ANS) [Tilmant et al. 2003] and the pupil size results from a balance of the separately incoming stimuli to the two muscles [Bergamin et al. 1998]. The ANS conducts the pupillary light reflex and *hippus* neural actions. Hippus are spontaneously irregular variations in pupil diameter, which can essentially be characterized as random noise in the 0.05 to 0.3 Hz frequency range [Stark 1939; Usui and Stark 1982]. In PLR, when light reaches the retina, neural signals are sent to the brain, which sends back a signal for closing or opening the pupil. Thus, PLR can be modeled in two phases: perception, and after some time delay, adjustment.

4. MODELS OF PUPIL DYNAMICS

The pupillometry literature describes several models built around experiments designed to measure the values of some parameters as a function of incident light intensity. Link and Stark [1988] performed a study where a light source was placed in front of the subjects' irises and, by varying the intensity and frequency of the light, they measured the pupillary latency (the time delay between the instant in which the light pulse reaches the retina and the beginning of iridal reaction):

$$\tau(R, L_{fL}) = 253 - 14\,ln(L_{fL}) + 70R - 29\,R\,ln(L_{fL}), \quad (1)$$

where τ is the latency in milliseconds, L_{fL} is the luminance measured in foot-Lamberts (fL), and R is the light frequency measured in Hz.

Other similar models predict an average pupil size as a function of the light intensity using a few experimental measurements [Moon and Spencer 1944; de Groot and Gebhard 1952; Pokorny and Smith 1997]. Among those, the most popular one is the Moon and Spencer model, which is expressed as:

$$D = 4.9 - 3tanh[0.4(log_{10}(L_b) - 0.5)], \quad (2)$$

where the pupil diameter, D, varies from 2 to 8 mm, and L_b is the background luminance level expressed in blondels, varying from 10^5 blondels in sunny days to 10^{-5} blondels in dark nights. $tanh$ is the hyperbolic tangent.

4.1 Physiologically-Based Models

In Mathematical Biology and related fields, models based on physiological and anatomical observations were derived to express the relationships among the pupillary action variables without relying on quantitative experimental data. For example, Usui and Stark [1982] proposed a parametric model of the iris to describe the static characteristics of pupil response to light stimuli, and to explain its random fluctuations in terms of probability density functions. Recently, Tilmant et al. [2003] proposed a model of PLR based on physiological knowledge and guided by experiments. Although they have obtained plausible results, Tilmant et al. have recommended the use of another physiologically-based model to more accurately monitor pupillary dynamics, namely the time-dependent model developed by Longtin and Milton [1989].

Longtin and Milton [1989] define the efferent neural signal $E(t)$ arriving at the iris per unit of time t, as:

$$E(t) = \beta\ ln\left[\frac{\phi(t-\tau)}{\bar{\phi}}\right], \quad (3)$$

where β is a constant of proportionality and ϕ is the retinal light flux measured in lumens and defined by Stark and Sherman [1959] as $\phi = I_l A$: illuminance (I_l, in lumens/mm^2) times the pupil area (A, in mm^2). τ is the latency, and $\bar{\phi}$ is the retinal light level threshold (the light level below which there is no change in the pupil area). The notation $\phi(t-\tau)$ indicates that the current effect depends on the retinal light flux at a time τ milliseconds in the past. As the efferent neural signal reaches the iris, it induces some muscular activity x that may cause the pupil to dilate or constrict. According to Partridge and Benton [1981], the relationship between $E(t)$ and x can be approximated by:

$$E(t) \tilde{=} k\left(\frac{dx}{dt} + \alpha x\right), \quad (4)$$

where k is a proportionality factor and α is a rate constant that depends on the definition and units of x used in the model. Longtin and Milton [1989] combine Equations (3) and (4) as:

$$\frac{dx}{dt} + \alpha x = \gamma\ ln\left[\frac{\phi(t-\tau)}{\bar{\phi}}\right]. \quad (5)$$

They express the pupil area as $A = f(x)$ and use the inverse $f^{-1}(A) = g(A) = x$ to remove x from Equation (5). In their paper, Longtin and Milton use a Hill function [Hill 1938] (Equation 6) as the function f, since it can approximate the elasto-mechanical properties of the iris during the pupillary activity:

$$A = f(x) = \frac{\Lambda\theta^n}{\theta^n + x^n} + \Lambda'. \quad (6)$$

Here, Λ' and $\Lambda + \Lambda'$ are, respectively, the minimum and the maximum pupil areas, and θ is the value of x corresponding to the average pupil area. Longtin and Milton's model then becomes:

$$\frac{dg}{dA}\frac{dA}{dt} + \alpha g(A) = \gamma\ ln\left[\frac{\phi(t-\tau)}{\bar{\phi}}\right], \quad (7)$$

where

$$g(A) = x = \sqrt[n]{\frac{\Lambda\theta^n}{A - \Lambda'} - \theta^n}. \quad (8)$$

An S-shaped curve similar to the Hill function has been described in the physiologically-based model of Usui and Stark [1982] to approximate the pupil diameter of an average individual under static illumination conditions.

5. THE PROPOSED PHYSIOLOGICAL-BASED MODEL

The model of Moon and Spencer (Equation (2)) is based on a set of discrete measurements and approximates the response on an average

individual under various lighting conditions. Their measurements were made after the pupil size had stabilized for each illumination level, and therefore, their model does not describe the pupil behavior outside the equilibrium state. Moreover, pupil size, latency, constriction, and redilation velocities tend to vary among individuals exposed to the same lighting stimulus [Moon and Spencer 1944; Winn et al. 1994]. We remark that such variations are not captured by the model of Moon and Spencer.

Longtin and Milton's model (Equation (7)) is time dependent and adaptive, with the potential to handle abrupt lighting changes. It is a theoretical model, and unfortunately, Longtin and Milton did not provide the values for the various parameters in their model (*i.e.*, γ, α, θ, n, $\bar{\phi}$), as these, in principle, depend on the abstract notion of iridal muscular activity x, as well as on the use of the Hill function. The use of incorrect parameter values will not produce realistic results and may cause Equation (7) to not converge.

Starting from Longtin and Milton's and from Moon and Spencer's models, we derive a practical model that predicts the pupil diameter for the nonequilibrium case based on experimental data (Section 5.2). In Section 5.3, we show how we can extend this basic model to take individual variability into account.

5.1 Equilibrium Case

Under constant lighting conditions, the pupil area in Longtin and Milton's model will converge to an equilibrium state, where:

$$\frac{dg}{dA}\frac{dA}{dt} = 0.$$

Under such a circumstance, and assuming there is no occurrence of hippus, ϕ becomes time invariant. Also, recall that $ln(m/n) = ln(m) - ln(n)$, and therefore, one can rewrite Longtin and Milton's model (Equation (7)) for the equilibrium case as:

$$\alpha g(A) = \gamma\ (ln(\phi) - ln(\bar{\phi})). \tag{9}$$

In turn, the Moon and Spencer model can be rewritten as

$$\left(\frac{D-4.9}{3}\right) = -tanh\left[0.4\left(\frac{ln(L_b)}{ln(10)} - 0.5\left(\frac{ln(10)}{ln(10)}\right)\right)\right],$$

and since the hyperbolic tangent is an odd function, we can rewrite this equation as:

$$-2.3026\ atanh\left(\frac{D-4.9}{3}\right) = 0.4(ln(L_b) - 1.1513), \tag{10}$$

where *atanh* is the arc-hyperbolic tangent. Comparing Equations (9) and (10), in order for Longtin and Milton's model to fit the response of Moon and Spencer's average subject under equilibrium conditions, one has:

$$-2.3026\ atanh\left(\frac{D-4.9}{3}\right) \approx \alpha g(A) \tag{11}$$

$$0.4(ln(L_b) - 1.1513) \approx \gamma(ln(\phi) - ln(\bar{\phi})). \tag{12}$$

From Equation (12) we can estimate the value of the parameter γ. One should note that L_b is expressed in blondels while ϕ is given in lumens. Although, in general one cannot convert between two photometric quantities, this can be done under some well-defined situations [Ohta and Robertson 2005]. Since Moon and Spencer's data were collected with the subject seated before a large white screen of uniform intensity which covers most of their field of view, we assume that the light reaching a person's pupil has been reflected by a perfect (Lambertian) diffuse surface. Recall that an ideal (lossless) diffuse reflector returns all of the incident flux so that its reflectance

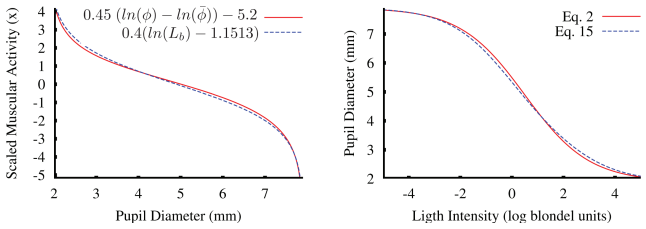

Fig. 2. High-quality fittings: (left) Both sides of Equation 13. (right) Equations 2 and 15, whose difference in absolute values is under 2% over the entire range $[10^{-5}, 10^5]$ blondels.

$\rho = 1$ and its BRDF $f = 1/\pi$ [Nicodemus et al. 1977]. For such a reflector, 1 blondel $= 10^{-6}$ lumens/mm^2 [Ohta and Robertson 2005].

Since the light flux, ϕ, depends on the area of the pupil, in order to estimate γ, we first evaluate the left-hand side of Equation (12) for the entire range of illumination covered by Moon and Spencer's model: $L_b \in [10^{-5}, 10^5]$ blondels. For each value of L_b, we then use Equation (2) to estimate D, from which the pupil area $A = \pi(D/2)^2$, and then ϕ, are computed. The retinal light level threshold $\bar{\phi} = 4.8118 \times 10^{-10}$ lumens was obtained using the pupil diameter $D_t = 7.8272$ mm, predicted by Equation 2 for $L_b = 10^{-5}$ blondels ($\bar{\phi} = \pi(7.8272/2)^2\ mm^2 \times 10^{-5}10^{-6}$ lumens/mm^2). Using the tabulated data for the left-hand side of Equation (12) and the conversion scheme just described, we get the following fitting:

$$0.4(ln(L_b) - 1.1513) \approx 0.45\ (ln(\phi) - ln(\bar{\phi})) - 5.2, \tag{13}$$

whose quality of approximation is illustrated in Figure 2 (left). The vertical axis of the graph (scaled muscular activity) represents $\alpha g(A)$, where $g(A) = x$ is the muscular activity. The extra constant -5.2 translates the function on the right-hand side of Equation 12 vertically, improving the fitting. Given Equation (13), we can replace $g(A)$ with $M(D)$ (Equation (11)), with $\alpha = -2.3026$, where $M(D)$ is given by:

$$M(D) = atanh\left(\frac{D-4.9}{3}\right). \tag{14}$$

Thus, the equilibrium situation can be expressed by Equation (15). As expected, it approximates Moon and Spencer's function (Equation (2)) for the pupil diameter of the average subject quite well. The absolute value of the difference between Equations (2) and (15) is under 2% over the entire range of $[10^{-5}, 10^5]$ blondels (Figure 2 right).

$$2.3026\ M(D) = 5.2 - 0.45\ ln\left[\frac{\phi}{\bar{\phi}}\right] \tag{15}$$

5.2 The Dynamic Case

Equation (15) cannot be used to describe the evolution of the pupil diameter in time as a function of instantaneous variations of the light intensity arriving at the pupil. Nevertheless, the obtained constants are still valid for the dynamic case, since the equilibrium is just a special case of the more general pupil behavior, for which the constants should also hold.

In general, one cannot take an equation obtained for equilibrium and generalize it to the dynamic case. In our model, however, this is possible because of the following constraints:

—$g(A)$ and $M(D)$ have no explicit time dependence;

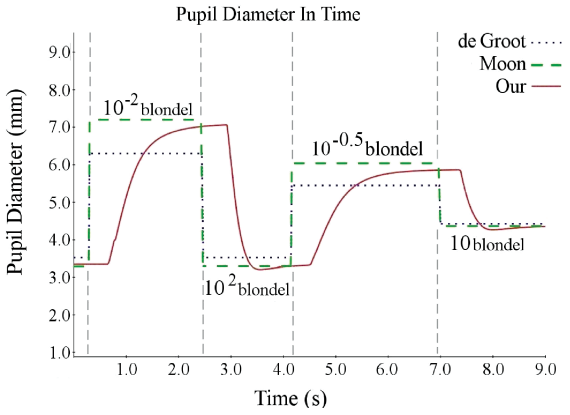

Fig. 3. Simulated results produced by our PLR model (Equation 16) for the average subject of Moon and Spencer under nonequilibrium conditions (solid line). For this simulation, the lighting assumed the following values: 10^{-2}, 10^{2}, $10^{-0.5}$, and 10 blondels, respectively (delimited by the vertical lines). These results are compared to the static models of Moon and Spencer [1944] (dashed line), and of De Groot and Gebhard [1952] (dotted line). Note the latency predicted by our model.

—the range of values assumed by A (or D) is the same for both the equilibrium and the nonequilibrium cases;

—there is a one-to-one mapping between A and D.

By introducing time in Equation (15), we obtain a delay differential equation that corresponds to our solution for the dynamic case:

$$\frac{dM}{dD}\frac{dD}{dt} + 2.3026\, atanh\left(\frac{D-4.9}{3}\right) = 5.2 - 0.45\, ln\left[\frac{\phi(t-\tau)}{\bar{\phi}}\right], \tag{16}$$

where D and ϕ are expressed in mm and lumens, respectively. For latency τ, we use Equation (1) noting that 1 blondel = 0.0929 fL. Pupil constriction velocity is approximately three times faster than (re)dilation velocity [Ellis 1981; Bergamin et al. 1998]. We take this difference into account by using different time steps for constriction (dt_c) and dilation (dt_d) in our numerical solver simulation:

$$dt_c = \frac{T_c - T_p}{S} \quad dt_d = \frac{T_c - T_p}{3S}, \tag{17}$$

where T_c and T_p are respectively the current and previous simulation times (times since the simulation started) measured in milliseconds, S is a constant that affects the constriction/dilation velocity and varies among individuals. The higher the S value, the smaller the time step used in the simulation and, consequently, the smaller the pupil constriction/dilation velocity.

Figure 3 shows pupil diameter values corresponding to Moon and Spencer's average subject simulated using Equation (16) considering some abrupt changes in the environment luminance. For this example, our results are compared to results provided by the static models of Moon and Spencer (Equation (2)) and of De Groot and Gebhard [1952]

5.3 Modeling Individual Differences

While Equation (16) simulates dynamic pupil behavior, it only does so for the average individual represented by the Moon and Spencer model. There are, however, substantial differences in the way pupils from different individuals react to a given light stimulus. Such variations include differences in diameter [Crawford 1936; Moon and Spencer 1944; de Groot and Gebhard 1952; Ellis 1981; Winn et al. 1994], latency, and constriction and redilation velocities [Ellis 1981; Bergamin et al. 1998]. In order to simulate individual differences, we cannot just arbitrarily change the parameter values of our model, as Equation (16) may not converge.

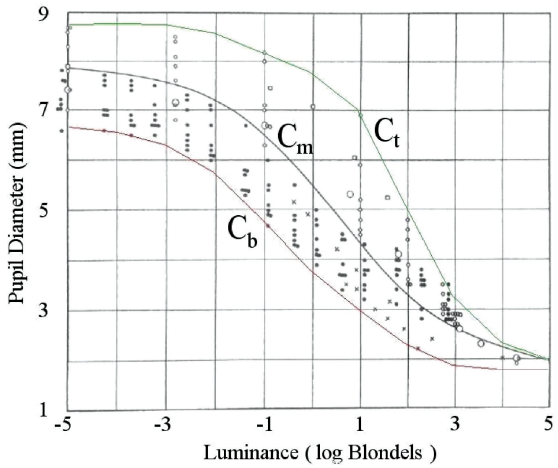

Fig. 4. Original data used by Moon and Spencer [1944]. The curve C_m corresponds to Equation 15. The pair of curves C_b and C_t define an envelope containing all data.

Figure 4 shows the original data used by Moon and Spencer [1944]. The curve C_m (shown in black), was obtained by converting the values of L_b in the range of $[10^{-5}, 10^{5}]$ blondels to lumens (see Section 5.1) and then using Equation (15) to compute the corresponding pupil diameter values used for plotting. The top and bottom curves, C_t and C_b, respectively, define an envelope containing all pupil diameter values used by Moon and Spencer. C_b was obtained by fitting a 5 degree polynomial to 11 of the smallest pupil diameter values along the entire luminance range. Likewise, C_t was obtained by fitting a 5 degree polynomial to 11 of the largest pupil diameter values. We treat C_b, C_m, and C_t as isocurves $C(p)$ for some parameter $p \in [0, 1]$, so that $C(0) = C_b$, and $C(1) = C_t$. We then model individual differences by associating to each individual I, an index $r_I \in [0, 1]$, which corresponds to an isocurve, $C(r_I)$. This index can be randomly generated or, alternatively, it can be recovered from experimental data as described in Section 5.4. To avoid convergence problems and still achieve the results corresponding to isocurve $C(r_I)$, we rewrite C_t and C_b, respectively, as new functions C_{tD} and C_{bD} of the pupil diameter:

$$\begin{aligned} C_{tD}(D) &= -0.013D^5 + 0.322D^4 - 3.096D^3 \\ &\quad + 13.655D^2 - 25.347D + 18.179 \end{aligned} \tag{18}$$

$$\begin{aligned} C_{bD}(D) &= -5.442D^5 + 1.387D^4 - 1.343D^3 \\ &\quad + 6.219D^2 - 1.317D + 1.219. \end{aligned} \tag{19}$$

In order to obtain C_{tD}, we evaluate the functions C_m and C_t for L_b in the range $[10^{-5}, 10^{5}]$ blondels, creating ordered pairs of diameter values $(D_m, D_t) = (C_m(L_b), C_t(L_b))$. Given enough of these pairs, we fit a curve expressing D_t as a function of D_m (or D for short). The resulting curve is C_{tD} (Equation (18)). The case of C_{bD} is similar. The final pupil diameter at any time is then obtained solving Equation 16 for D and then evaluating:

$$D_{final} = C_{bD}(D) + (C_{tD}(D) - C_{bD}(D))r_I. \tag{20}$$

We have adopted this solution due to its simplicity and generality: we can easily replace the curves $C_{bD}(D)$ and $C_{tD}(D)$ with new ones, covering new data as they become available, or representing other models (e.g., De Groot and Gebhard [1952]). Since the relative distances of C_m to C_b and C_t vary for different values of D, no value of r_I will exactly recover C_m. This is not a problem, however, as C_m corresponds to the average subject. Other parameterizations are possible, including ones that interpolate C_m for a given value of r_I.

Although our model properly simulates the elastic behavior of the iris muscular activity during changes in lighting conditions, it does not model hippus (Equation 16 will converge to some pupil diameter value if the lighting conditions remain constant). As random fluctuations whose causes are still unknown [Usui and Stark 1982; Ukai et al. 1997], it is currently not possible to define a physiologically-based model for hippus. We visually approximate the hippus effect by adding small random variations to the light intensity (between $-10^{0.3}$ and $10^{0.3}$ blondels), to induce small variations in the pupil diameter (of the order of 0.2 mm [Hachol et al. 2007]), in the frequency range of 0.05Hz to 0.3Hz. This significantly improves the realism of the resulting simulations and animations. According to Usui and Stark [1982], the standard deviation of the noise corresponds to approximately 10% of the pupil diameter.

5.4 The PLR Model Validation

In order to validate our PLR model under nonequilibrium conditions and to show that it is capable of representing individual variability, we performed some qualitative comparisons between actual pupil behavior and the results of simulations produced by our model. For this, we captured videos of normal subjects presenting significantly different light sensitivities (different PLR responses), while a light was turned on and off several times. Since pupil constriction is bigger when both eyes are stimulated [Thomson 1947], the subjects kept both eyes opened. To avoid fatigue and habituation of the iris [Lowenstein and Loewenfeld 1964], in each experiment we recorded less than one minute of video per subject.

We computed the pupil diameters of the subjects at each frame of the video sequences. Lighting measurements made during video capture were used as input to our PLR model for simulating pupil behavior. The pupil diameters resulting from these simulations were then compared to the pupil diameters computed at individual video frames. Note that the simulated results are not expected to quantitatively match the observed ones, but rather be in qualitative agreement with observed behavior.

The videos were captured using a Cannon ELURA2 miniDV camcorder (NTSC, 720×576 pixels) with progressive scan, connected to a PC through a firewire connection. We kept the room's light dimmed so that the subjects' pupils could dilate naturally to some extent, but not so dark that we could not see the pupils in the individual video frames. Because of these constraints, we used two subjects (both males) with light eyes (a 24-year-old with green eyes, and a 26-year-old with blue eyes). For each frame, the pupil diameters were estimated from the set of dark pixels (pupil area P_{area}) inside a specified rectangle containing solely the subject's pupil and part of the iris (Figure 5). Given P_{area}, the pupil diameter was obtained (assuming the pupil is a circle) as $d = 2(\sqrt{P_{area}/\pi})$ pixels. The conversion from pixels to millimeters was performed considering a typical iris diameter of 12mm. According to our experience, computing the pupil diameter as described produces more accurate results than computing it as the number of pixels in the largest straight segment in the set of dark pixels (the pupil).

Since the video frames were captured at approximately 30Hz, in practice no variation is expected between the pupil diameters in neighbor frames under constant illumination, even in the presence of hippus. Thus, we estimated the average error in the computed pupil diameters to be approximately 0.1mm by computing the average difference between estimated pupil diameters for neighbor frames. Based on the video sequences, we set $S = 600$ (Equation (17)) for the two subjects in all experiments, as this value made their simulated constriction velocities approximate the ones in the video sequences. We empirically set the frequency of the two light sources used in our experiments to $R = 0.4$Hz, a value that made the latency estimated by Equation (1) approximate the latency observed in the video frames.

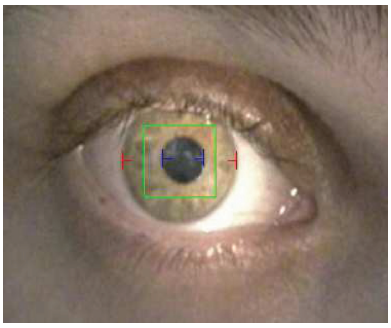

Fig. 5. Estimating pupil diameter from a rectangular region containing only the pupil and some iris pixels. The pupil diameter is estimated from the area occupied by the dark pixels, assuming a circular pupil and an iris with diameter of 12mm.

To evaluate the quality of our simulations, we performed experiments with both subjects using two different kinds of light sources to induce pupil constriction: a small flashlight and a 100-watt incandescent white light bulb. For light measurements, we used an LD-200 Instrutemp digital lux meter (precision ±3%, frequency 2 Hz).

5.4.1 *The Flashlight Experiments.* In these experiments, we used a light source to induce significant changes in the subjects' pupil diameters without introducing considerable changes in the lighting conditions of the environment. For this purpose, we used a small flashlight powered by a single AAA battery (1.5 Volt) kept at about 20cm from the subject's right eye and pointed at it. Given the small area illuminated by the flashlight as well as its reduced power, the readings from the lux meter were very sensitive to even small changes in the relative position and orientation of the flashlight with respect to lux meter sensor. Thus, we decided to run two simulations using the recorded data: (1) considering the light intensity estimated using Equation (2), and (2) considering the readings from the lux meter. These two experiments are explained next.

The first flashlight experiment. In this experiment, we used the Moon and Spencer equation (Equation (2)) to solve for the light intensities during the on and off states of the flashlight, based on the measured pupil diameters (from the video). Since the Moon and Spencer function (curve C_m in Figure 4) represents the pupil behavior of an average individual, we estimated the on (off) light intensity as the average of the computed on (off) intensities for both subjects. Using this procedure, we obtained estimates of $10^{1.1}$ blondels when the flashlight was on, and $10^{-0.5}$ blondels when the flashlight was off. Given the average luminance value for the on (off) state and the corresponding pupil diameter for a given subject, we used Equation (20) to estimate the $r_{I_{on}}$ ($r_{I_{off}}$) index for that subject. The

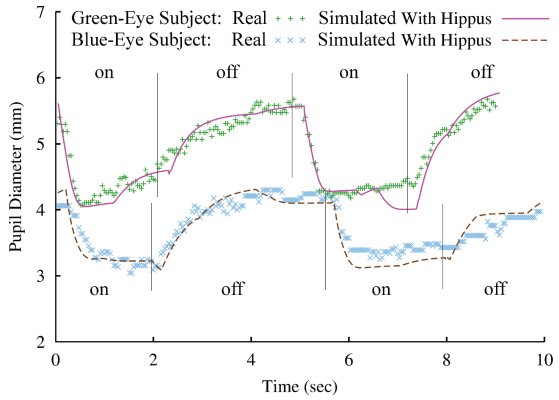

Fig. 6. Comparison between our simulated results and measurements from real video sequences using the flashlight as stimulus. The green "+" and the blue "x" marks represent, respectively, the pupil diameter measurements for the green-eye and for the blue-eye subjects, obtained for all frames along a 9-second-long video sequence. The solid and dashed lines are the pupil diameters predicted by our physiologically-based model for the green-eye and for the blue-eye subjects, respectively, after random noise (hippus effect) has been added. The vertical dotted lines delimit the intervals in which the flashlight was kept on and off for each subject. The predicted values closely agree with the actual measured values.

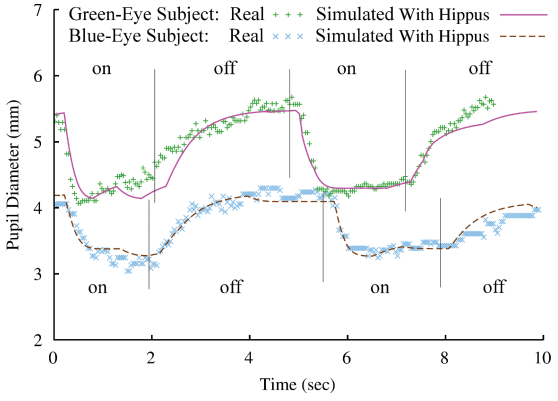

Fig. 7. Similar to the graphs shown in Figure 6 but using the illuminance readings provided by the lux meter as input to our model. The simulated results, including hippus, for the green-eye and blue-eye subjects are shown as solid and dashed lines, respectively.

subject's final r_I index was computed as the average between his $r_{I_{on}}$ and $r_{I_{off}}$ indices. Using this procedure, we obtained $r_I = 0.4$ for the green-eye subject and $r_I = 0.03$ for the blue-eye subject.

Figure 6 shows the actual pupil diameter measurements performed on a frame-by-frame basis along 9-second-long sequences captured for each subject. The green "+" marks on top represent the measurements for the green-eye subject, while the blue "x" marks show the measurements of the blue-eye subject. This example illustrates the intersubject variability in terms of light sensitivity and shows the ability of our model to appropriately represent such individual differences. The vertical dotted lines delimit the intervals in which the flashlight was kept on and off for each subject. The solid and dashed lines represent the simulated results produced by our model for the green-eye and blue-eye subjects, respectively, and closely agree with the actual measured values. These curves were produced automatically from Equations (16) and (20), on top of which we added small random variations (hippus effect) as described in the previous section. The accompanying video shows side-by-side comparisons of our simulated results and videos captured for the two subjects.

The second flashlight experiment. In this experiment, we used the readings provided by the lux meter for the on and off states of the flashlight. These illuminance values were 350lux[1] and 90lux, respectively. One should recall that in such a setup, small changes in the position and orientation of the subject's head produce changes in the illuminance at the pupil. Therefore, these values are only approximations to the actual illuminance reaching each subject's lit eye. Given the illuminance values and the subjects' corresponding pupil diameters estimated from the video frames, we obtained the actual pupil's luminous flux (in lumens) at the two flashlight states, for each individual. These values were then converted to blondels according to the assumption described in Section 5.1. We then used Equations (16) and (20) to estimate their corresponding r_I indices (by averaging $r_{I_{on}}$ and $r_{I_{off}}$), obtaining $r_I = 0.54$ for the blue-eye subject and $r_I = 0.92$ for the green-eye subject. Figure 7 compares the actual pupil measurements (same as in Figure 6) with the results simulated by our model using the lux meter readings as input. The differences between the simulated curves shown in Figures 6 and 7 are primarily due to the added random noise (hippus).

5.4.2 *The 100-Watt Lightbulb Experiment.* For this experiment we used a more stable light source to induce pupil constriction: a spot with a 100-watt incandescent white lightbulb, kept at about one meter in front and one meter to the right of the subject's head. This setup allowed the subjects to remain comfortable with their eyes opened while the light was on.

We measured the environment light intensity during the on and off states by positioning the digital lux meter at approximately the same position and orientation as the subject's right eye. During the blue-eye subject experiment, we found the illuminance to be equal to 140 lux when the light was off and 315 lux when it was on. During the green-eye subject experiment, the readings were 91 and 540 lux, respectively. These differences resulted from a darker environment and a slight approximation of the green-eye subject to the light source. Again, we used the illuminance values and the subjects' corresponding pupil diameters (measured from the video) as input to Equations (16) and (20) to estimate their corresponding r_I indices (by averaging $r_{I_{on}}$ and $r_{I_{off}}$). We obtained $r_I = 0.9$ for the blue-eye subject and $r_I = 1.0$ for the green-eye subject.

Figure 8 (top) shows the actual pupil diameter measurements performed on a frame-by-frame basis along 56- and 50-second-long sequences captured for the blue-eye and for the green-eye subjects, respectively. The vertical lines delimit the intervals in which the light was kept on and off for each subject. The solid and dashed lines represent the simulated results produced automatically by our model (Equations 16 and 20) with and without hippus, respectively, and closely agree with the actual measurements. Figure 8 (bottom) shows zoomed versions of portions of the graphs shown on top, exhibiting off-on-off transitions.

One should note that the simulated results produced by our PLR model closely approximate the actual behaviors of the subjects' pupils in all three experiments, illustrating the effectiveness of our model. The differences in the r_I indices for a given subject among the experiments can be explained as follows.

—In the two flashlight experiments, the pupil diameters used for the on and off states were the same, but the illuminance values

[1] $1\ lux = 1\ lumen/m^2$

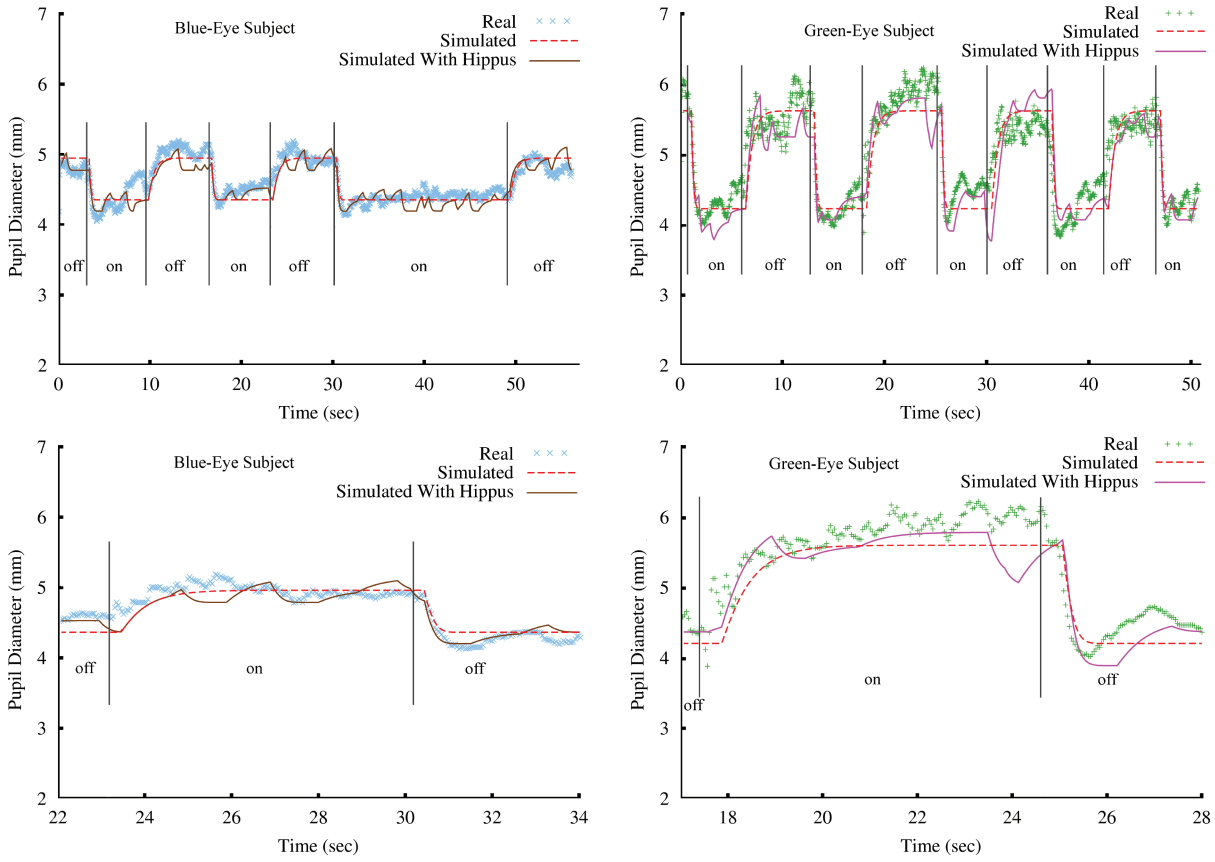

Fig. 8. Comparison between our simulated results and measurements from real video sequences using light emitted by a lightbulb as stimulus. The "x" and "+" marks represent the pupil diameter measurements for the blue-eye (left), and for the green-eye (right) subjects, respectively. Top row: values obtained for all frames along 56- and 50-second-long video sequences, respectively. The solid and dashed lines are the pupil diameters predicted by our physiologically-based model with and without hippus, respectively. The vertical lines delimit the intervals in which the incandescent light bulb was kept on and off for each subject. The predicted values match the actual measurements well. The bottom row shows zoomed versions of the graphs shown on the top.

provided by Equation 2 and by the lux meter were different. The different indices simply reflect the different light sensitivities presented to our model as input.

—When comparing the 100-watt lightbulb and the flashlight experiments, both the lighting and the pupil sizes varied for the on and off states of the light sources. For instance, for the green-eye subject, the pupil diameters were approximately 4.3mm and 5.7mm for the on and off states of the flashlight, respectively (Figure 7). This resulted in an r_I index of 0.92. In the case of the 100-watt lightbulb experiment, these values were approximately 4.3mm and 6.0mm, respectively (Figure 8), with $r_I = 1.0$. These two indices are relatively close and reflect the difference in the maximum pupil diameters between the two experiments. The difference in the r_I indices for the blue-eye subject were considerably larger, from 0.54 to 0.9. Again, this can be explained by comparing the measured pupil diameters in the two experiments. These values went from approximately 3.2mm and 4.2mm in the on and off states of the flashlight (Figure 7) to 4.4mm and 5.2mm in the on and off states of the 100-watt lightbulb (Figure 8).

An important point to note is that by using an average of the estimated r_I indices for the on and off states of the light source, our model is capable of realistically simulating the pupil behavior of individuals with considerable differences in PLR responses under different and variable lighting conditions.

6. MODELING THE IRIS DEFORMATION

Although the iris is a well-known structure [Freddo 1996], there is no general agreement about a model of its behavior. Rohen [1951] seems to have been the first researcher to study the form of the collagen structure of the iris. He suggested that the collagen fibers are arranged in a series of parallel arcs, connecting the iris root with the pupil border, clockwise and counterclockwise in an angle of 90 degrees oriented by the center of the pupil. These fibers would be interwoven with other iris components, such as blood vessels. Based on Rohen's fiber arrangement, Wyatt [2000] proposed a 2D nonlinear model for iris deformation. Such a model has been validated on canine, porcine, and monkey irises, but so far not on human irises [Wyatt private communication].

We derived our model for iridal pattern deformation by analyzing sets of photographs taken from five volunteers under controlled conditions. In our experiments, an eye doctor dilated their pupils with some mydriatic drug and we photographed their irises at several stages during the pupil dilatation process using a Canon PowerShot SD 400 camera with macro lens. The images were taken

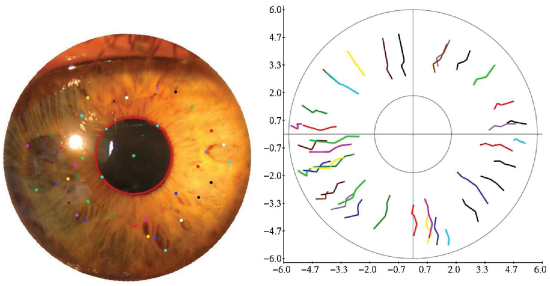

Fig. 9. Left: Photograph of a volunteer's iris taken during the dilation process. The colored dots indicate tracked feature points and the center of the pupil. Right: Evolution of the positions of the individually tracked points during the dilation process. Each feature point is identified by a different color.

at a resolution of 2048 × 1536 pixels, and were then cropped to square images containing only the iris and pupil. After cropping, the smallest image was 800 × 800 pixels and the larger ones were rescaled to fit the same dimensions. Thus, let $S_i = \{I_{i1}, I_{i2}, ..., I_{in}\}$ be the set of n images from a given volunteer V_i taken along the pupil dilation process. For each image I_{ij}, we positioned a circle on the outer border of the iris and another one at the border of the pupil (the two circles delimit the iridal disk). We also defined the center of the pupil as the center of the inner circle. We then manually marked a series of iridal feature points and tracked them along the set of images of each volunteer. Figure 9 (left) shows an image with the tracked features indicated by a set of colored dots. The complete set of images used for tracking the iridal features of this volunteer is shown in Figure 10.

Figure 9 (right) shows how the positions of the individually tracked iridal feature points changed along the dilation process. The trajectories of the points both on the pupillary and ciliary zones move on approximately radial paths. Although some imprecision in the exact location of the points might have resulted from the manual specification, most of the deviation from the radial paths result from the existence of blood vessels under the iris, and from crypts, and folds (the iris folds its tissue as a result of pupil dilation) that prevent iris points from always moving along radial lines. Such structures vary considerably among individuals but, according to our experience, their influence on the paths of the feature points usually has small magnitude (Figure 9 right). Therefore, as a first approximation, we can assume that the iris points move along straight lines in the radial directions. It is worth noting that Wyatt's 2D model [Wyatt 2000] does not take the influence of these structures into account either.

In order to find how fast the feature points moved, we computed the following measures during the dilation process: (1) the distance from the tracked feature point to the pupil center; (2) the distance from the tracked feature point to the pupil border; and (3) the ratio between the distance from the tracked point to the pupil border and the local width of the iridal disk (the distance from the pupil border to the external iris border measured along the radial segment passing through the feature point). One should recall that the pupil is not necessarily circular and that its center does not necessarily coincide with the center of the iris. While measurements (1) and (2) presented a pretty much linear behavior, the ratio represented by (3) was approximately constant for all feature points (Figure 10 right). The same behavior was observed in the irises of all five volunteers. Like the variations in the trajectories of the points shown in Figure 9 (right), the deviations from horizontal lines in Figure 10 (right) are caused by the subjects' iris structures, specially the iridal folds. Again, as a first approximation, the following ratio can be assumed constant for any iridal point p_i, for all values of pupil diameters:

$$\rho_i = \frac{\|p_i - c_i\|}{\|E_i - c_i\|}, \tag{21}$$

where p_i is a point on the iris disk, c_i and E_i are the points on the pupil border and on the iris outer circle, respectively, such that they are collinear to the radial segment passing through p_i. $\|.\|$ is the L^2 (Euclidean) norm. The invariance expressed by Equation 21 summarizes the observations illustrated in Figure 10 (right) and is the basis of our image-based model for iridal pattern deformation.

6.1 Animating the Deformed Iridal Patterns

As an approximation to the behaviors depicted in Figures 9 (right) and 10 (right), we use texture mapping to animate the iris deformation process. Note that this is a natural and efficient way of implementing the behavior modeled by Equation (21): as the pupil dilates/constricts, the iris ring is compressed/stretched, but the parameterization (in the [0, 1] × [0, 1] domain) of the points inside the ring remains the same. Thus, for animation purposes, we model the iris as a planar triangle-strip mesh on the disk defined by the two circles with a small pupil diameter as a texture. Texture coordinates map the border of the pupil to the inner circle of the mesh, and outer border of the iris to the mesh's outer circle. Currently, we tessellate the mesh creating a pair of triangles at every five degrees. The animation proceeds by computing the new pupil diameter D as a function of the incident lighting using Equation (20). We then reposition each vertex v_i, located on the inner circle of the mesh, at a distance $D/2$ along the radial line connecting the center of the pupil to v_i, while keeping their original texture coordinates unchanged. One should recall that the center of the pupil does not necessarily match the center of the iris, and thus, it is important to keep the coordinates of the center of the pupil. Figure 11 shows the renderings of an iris created using our models for different lighting conditions. Note that the patterns deform in a natural way. No light reflection on a corneal surface has been simulated, to avoid masking iris details. Figure 12 compares the results produced by our models with actual photographs. Note that the deformed patterns closely approximate the ones in the photographs.

7. DISCUSSION

We have implemented the proposed models and used them to render synthetic images of the human iris and pupil. The resulting animations are very convincing and run in real time. We have compared the images produced by our models with photographs and videos of real human irises. The results produced by our models are in qualitative agreement with observed behavior in humans.

In order to demonstrate the potential use of the proposed models in computer graphics, we built an application that renders a human head model in an environment illuminated by HDR cube maps (see accompanying video). The head model was obtained from Turbo Squid [2007] and its original irises were replaced by our textured triangle-strip model. The HDR images were obtained from Paul Debevec's web site [Debevec 2007] and are used to approximate the environment's radiance. As the head looks at different parts of the environment, its pupil diameters adapt to the irradiance in the solid angle defined by its field of view, producing pleasing animation effects.

Accommodation and age affect the pupil diameter [Winn et al. 1994] and iris color influences some PLR parameters, such

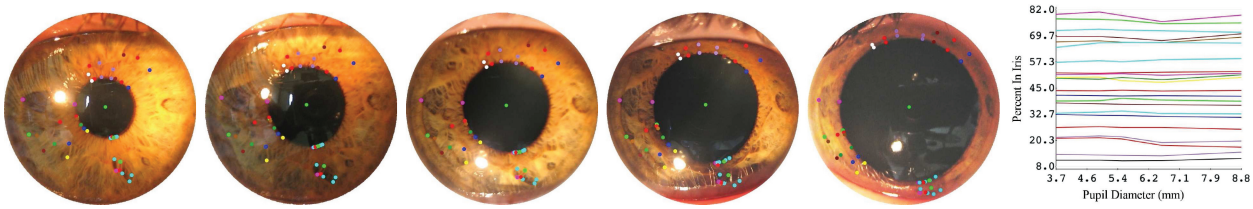

Fig. 10. Set of images used to track the iridal features of a volunteer along the dilation process. Color dots indicate corresponding points in the different images. From left to right, the pupil diameter values are: 3.70, 4.94, 5.53, 6.57, and 8.81mm, respectively. The apparent changes in iris color are due to the changes in the position of the light source used to illuminate the subject's eye (the camera's flash was turned off). The graph on the right shows evolution of the ratio defined by Equation (21) for all tracked feature points along the dilation process. The graph shows 22 out of 50 tracked points for one subject (due to space constraints). This pattern of an approximately constant ratio was observed for all subjects and all tracked points.

Fig. 11. Examples of iris rendered using our PLR and iridal pattern deformation models. Images simulated for light intensities of 10^5 blondels (left) and 1 blondel (right), for the Moon and Spencer's average subject. Note that the pupil is offset from the center of the iris disk. No light reflection on the corneal surface has been simulated to avoid masking iris details.

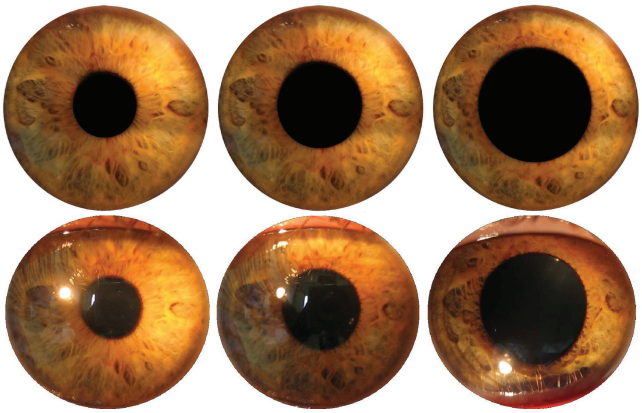

Fig. 12. Comparison of our simulated results with a set of photographs. Top: renderings produced using our pupil light reflex and iridal pattern deformation models for environments with 35,638.7, 3,102.52, and 71.85 lumens/mm^2, respectively. No light reflection on the corneal surface has been simulated to avoid masking iris details. Bottom: photographs of a human iris. Note the realistic deformation of the iridal patterns.

as maximum pupil diameter, latency, and constriction velocity [Bergamin et al. 1998]. These aspects are currently not taken into account by our model because of the lack of reliable data over a large range of lighting conditions. For instance, Winn et al. [1994] discuss the effect of age on the size of the pupil. Their study, however, only considered luminance values from 10^1 to 10^4 blondels, which corresponds to only about 30% of the luminance range used by our model. Currently, we model variations in pupil diameters for the same light stimulus using Equation 20, which can be used to simulate the age-related miosis effect reported by Winn. Also, since our model covers the entire range of valid pupil diameter values, it safely covers the pupillary sizes resulting from influence of attentional and other cognitive factors. Extending our model to handle other phenomena based on biophysical parameters is an interesting direction for future work.

No relief data representing the iris folds are used in the current version of the model, as it is done in the technique presented by François et al. [2007]. Also, no corneal refraction is used. Thus, at grazing angles, in addition to the distortion resulting from pupil dilation/constriction, one would perceive the projective distortion due to texture mapping. Relief information could be added to our model in a straightforward way, allowing some interesting shading effects such as projected shadows and self-occlusions [Policarpo et al. 2005; Oliveira and Policarpo 2005].

We use a linear model for iridal pattern deformation even though the actual deformation is nonlinear. However, according to Wyatt [2000], such nonlinearity contributes approximately only 1% of the diameter of a typical iris (12.0mm). Most of the nonlinear behavior seen in Figure 9 (right) and Figure 10 (right) is due to the interference of folds and blood vessels, which varies among individuals. To the best of our knowledge, no model in the literature takes those factors into account.

Many other factors affect pupil size [Tryon 1975], including particular states of mind, such as interest and curiosity [Hess and Polt 1964], spectral sensitivity [Werner 2003], respiratory and heart rate [Calcagnini et al. 2000], and spatial patterns in the visual field [Li et al. 2006]. Taking all these aspects into account seems to be impractical due to their inherent complexity and limited supporting data. We should emphasize that PLR causes the single most noticeable involuntary movements of the pupil. As the graphs depicted in Figures 7 and 8 and the accompanying video show, our PLR model alone can produce predictable animations of the pupil dynamics.

8. CONCLUSION

We have presented new models for realistic renderings of the human iris and pupil. Our physiologically-based model of the pupil light reflex combines and extends theoretical results from the Mathematical Biology field [Longtin and Milton 1989] with experimental data collected by several researchers [Moon and Spencer 1944]. The resulting model is expressed in terms of a nonlinear delay-differential equation that describes the changes in the pupil diameter as function of the environment lighting. Our model is also original in the sense that it can simulate individual differences with respect to light sensitivity. As all parameters of our models were derived from experimental data, they correctly simulate the actual behavior of the

human iris and pupil. They also produce high-fidelity appearance effects, which can be used to create real-time predictive animations of the pupil and iris under variable lighting conditions. We have validated our models through comparisons of our simulated results against videos and photographs captured from human irises. The quality of these simulations qualitatively matched the actual behaviors of human pupils and irises.

To the best of our knowledge, ours is the first physiologically-based model for simulating pupil light reflex presented in the graphics literature. It is also the first practical model (providing actual coefficient values) in the literature for simulating the dynamics of pupil and iris under variable lighting conditions, and the first integrated model in all of the literature to consider individual variability in pupil diameter using general equations for latency and velocity. Our image-based model for iridal pattern deformation is also the first model of its kind in the graphics literature. Our results should find applicability in several areas requiring high-fidelity facial animations, as well as on feature film animations, where the request for increasing levels of realism never ends.

We believe that this work can also contribute to investigations outside the scope of computer graphics. More specifically, the simulation tools presented in this article can be used to complement wet experiments and accelerate the hypothesis evaluation cycle in ophthalmological and physiological research. It is worth mentioning that computer simulations are being successfully and routinely used by biologists and medical researchers to study the predictive behavior of living systems under various conditions, including some not yet experimentally tested [Ventura et al. 2006].

ACKNOWLEDGMENTS

We are grateful to the following people for resources, discussions and suggestions: Prof. Jacobo Melamed Cattan (Ophthalmology-UFRGS), Prof. Roberto da Silva (UFRGS), Prof. Luis A. V. Carvalho (Optics-USP/SC), Prof. Anatolio Laschuk (UFRGS), Leandro Fernandes, Marcos Slomp, Leandro Lichtenfelz, Renato Silveira, Eduardo Gastal, and Denison Tavares. We also thank the volunteers who allowed us to collect pictures and videos of their irises: Alex Gimenes, Boris Starov, Christian Pagot, Claudio Menezes, Giovane Kuhn, João Paulo Gois, Leonardo Schmitz, Rodrigo Mendes, and Tiago Etiene.

REFERENCES

BERGAMIN, O., SCHOETZAU, A., SUGIMOTO, K., AND ZULAUF, M. 1998. The influence of iris color on the pupillary light reflex. *Graefes Arch Clin Exp Ophthalmol 236*, 8, 567–570.

CALCAGNINI, G., CENSI, F., LINO, S., AND CERUTTI, S. 2000. Spontaneous fluctuations of human pupil reflect central autonomic rhythms. *Methods Inf. Med. 39*, 2, 142–145.

CRAWFORD, B. H. 1936. The integration of the glare effects from a number of glare sources. *Proc. Phys. Soc. 48*, 1, 35–37.

CUI, J., WANG, Y., HUANG, J., TAN, T., AND SUN, Z. 2004. An iris image synthesis method based on PCA and super-resolution. In *Proceedings of the 17th International Conference of Pattern Recognition (ICPR)*. 471–474.

DE GROOT, S. G. AND GEBHARD, J. W. 1952. Pupil size as determined by adapting luminance. *J. Opt. Soc. Am. 42*, 492–495.

DEBEVEC, P. 2007. Paul debevec homepage. `http://www.debevec.org/`.

ELLIS, C. J. 1981. The pupillary light reflex in normal subjects. *Brit. J. Ophthal. 65*, 11, 754–759.

FERWERDA, J. 2003. Three varieties of realism in computer graphics. In *Proceedings of SPIE Human Vision and Electronic Imaging*. The International Society for Optical Engineering, 290–297.

FRANÇOIS, G., GAUTRON, P., BRETON, G., AND BOUATOUCH, K. 2007. Anatomically accurate modeling and rendering of the human eye. In *Special Interest Group on Graphics and Interactive Techniques (SIGGRAPH): Sketches*. ACM, New York, 59.

FREDDO, T. 1996. Ultrastructure of the iris. *Micros. Res. Tech. 33*, 369–389.

HACHOL, A., SZCZEPANOWSKA-NOWAK, W., KASPRZAK, H., ZAWOJSKA, I., DUDZINSKI, A., KINASZ, R., AND WYGLEDOWSKA-PROMIENSKA, D. 2007. Measurement of pupil reactivity using fast pupillometry. *Physiol. Meas. 28*, 61–72.

HESS, E. H. AND POLT, J. M. 1964. Pupil size in relation to mental activity during simple problem-solving. *Science 143*, 1190–1192.

HILL, A. V. 1938. The heat of shortening and the dynamic constants of muscle. *Proc. R. Soc. London B. Biol. Sci. 126*, 136–195.

LAM, M. W. Y. AND BARANOSKI, G. V. G. 2006. A predictive light transport model for the human iris. *Comput. Graph. Forum 25*, 3, 359–368.

LEE, S., BADLER, J., AND BADLER, N. 2002. Eyes alive. *ACM Trans. Graph. 21,* 3, 637–644.

LEFOHN, A., BUDGE, B., SHIRLEY, P., CARUSO, R., AND REINHARD, E. 2003. An oculariست's approach to human iris synthesis. *IEEE Comput. Graph. Appl. 23,* 6, 70–75.

LI, Z., LIANG, P., AND SUN, F. 2006. Properties of pupillary responses to dynamic random-dot stereograms. *Exp. Brain Res. 168*, 436–440.

LINK, N. AND STARK, L. 1988. Latency of the pupillary response. *IEEE Trans. Bio. Eng. 35*, 3, 214–218.

LONGTIN, A. AND MILTON, J. G. 1989. Modelling autonomous oscilations in the human pupil light reflex using nonlinear delay-differential equations. *Bull. Math. Bio. 51*, 5, 605– 624.

LOWENSTEIN, O. AND LOEWENFELD, I. E. 1964. The sleep-waking cycle and pupillary activity. *Annals NY Acad. Sci. 117*, 142–156.

MAKTHAL, S. AND ROSS, A. 2005. Synthesis of iris images using Markov random fields. In *Proceedings of the European Signal Processing Conference (EUSIPCO)*.

MOON, P. AND SPENCER, D. 1944. On the Stiles-Crawford Effect. *J. Opt. Soc. Am. 34*, 319–329.

NEWSOME, D. AND LOEWENFELD, I. 1971. Iris mechanics. ii. influence of pupil size on dynamics of pupillary movements. *Am. J. Ophthalmol. 71,* 1 Part 2, 353–373.

NICODEMUS, F. E., RICHMOND, J. C., HSIA, J. J., GINSBERG, I. W., AND LIMPERIS, T. 1977. Geometrical considerations and nomenclature for reflectance. Tech. Rep., Institute for Basic Stds. (Oct). National Bureau of Stds, Washington, DC.

OHTA, N. AND ROBERTSON, A. 2005. *Colorimetry: Fundamentals and Applications*. John Wiley & Sons, New York.

OLIVEIRA, M. M. AND POLICARPO, F. 2005. An efficient representation for surface details. Tech. rep. RP-351, UFRGS, Porto Alegre, Brazil.

PARTRIDGE, L. D. AND BENTON, L. A. 1981. *Handbook of Physiology, Motor Control*. Vol. 2. Chapter Muscle: The Motor. American Physiological Society, Washington, 43–106.

POKORNY, J. AND SMITH, V. C. 1997. The verriest lecture. How much light reaches the retina? In C.R. Cavonius, Ed. *Colour Vision Deficiencies XIII. Doc. Ophth. Proc. Series 59*. 491–511.

POLICARPO, F., OLIVEIRA, M. M., AND COMBA, J. L. D. 2005. Real-time relief mapping on arbitrary polygonal surfaces. In *Proceedings of the Symposium on Interactive 3D Graphics and Games*. ACM, New York, NY, 155–162.

REEVES, P. 1920. The response of the average pupil to various intensities of light. *J. Opt. Soc. Am. 4*, 2, 35–43.

ROHEN. 1951. Der bau der regenbogenhaut beim menschen und einigen sÔugern. *Gegenbaur Morphology J. 91*, 140–181.

SAGAR, M., BULLIVANT, D., MALLINSON, G., HUNTER, P., AND HUNTER, I. 1994. A virtual environment and model of the eye for surgical simulation. In *Proceedings of the Special Interest Group on Graphics and Interactive Techniques (SIGGRAPH)*, Annual Conference Series.

STARK, L. W. 1939. Stability, oscillations, and noise in the human pupil servomechanism. *Proc. IRE 47*, 11, 1925–1939.

STARK, L. W. AND SHERMAN, P. M. 1959. A servoanalytic study of consensual pupil reflex to light. *J. Neurophysiol. 20*, 17–26.

THOMSON, L. C. 1947. Binocular summation within the nervous pathways of the PLR. *J. Physiology 106*, 59–65.

TILMANT, C., CHARAVEL, M., PONROUCH, M., GINDRE, G., SARRY, L., AND BOIRE, J.-Y. 2003. Monitoring and modeling of pupillary dynamics. *Proceedings of 25th IEEE EMBS 1*, 678– 681.

TREVOR-ROPER, P. D. AND CURRAN, P. V. 1984. *The Eye and Its Disorders*. Vol. 3. Chapter The Eyeball. Blackwell Scientific Publications, Oxford, UK, 3–75.

TRYON, W. W. 1975. Pupillometry: A survey of sources of variation. *Psychophysiology 12,* 1, 90–93.

TURBO SQUID. 2007. 3d max male face head. `http://www.turbosquid.com/FullPreview/Index.cfm/ID/357993`.

UKAI, K., TSUCHIYA, K., AND ISHIKAWA, S. 1997. Induced pupillary hippus following near vision: increased occurrence in visual display unit workers. *Ergonomics 40,* 11, 1201–1211.

USUI, S. AND STARK, L. 1982. A model for nonlinear stochastic behavior of the pupil. *BioCyber 45,* 1, 13–21.

VENTURA, B., LEMERLE, C., MICHALODIMITRAKIS, K., AND SERRANO, L. 2006. From *in vivo* to *in silico* biology and back. *Nature 443*, 527–533.

WATT, A. AND WATT, M. 1992. *Advanced Animation and Rendering Techniques*. Addison-Wesley, New York.

WECKER, L., SAMAVATI, F., AND GAVRILOVA, M. 2005. Iris synthesis: a reverse subdivision application. In *Proceedings of the International Conference on Computer Graphics and Interactive Techniques (GRAPHITE)*, 121–125.

WERNER, A. 2003. Spectral sensitivity of the pupillary system. *Clin. Exp. Optom. 86*, 4, 235–238.

WINN, B., WHITAKER, D., ELLIOTT, D. B., AND PHILLIPS, N. J. 1994. Factors affecting light-adapted pupil size in normal human subjects. *Invest. Opthmol. Vis. Sci. 35*, 3.

WYATT, H. J. 2000. A minimum-wear-and-tear meshwork for the iris. *Vision Res. 40*, 2167–2176.

ZUO, J. AND SCHMID, N. A. 2005. A model based, anatomy based method for synthesizing iris images. In *Proceedings of IAPR International Conference on Biometrics*. 428–435.

Received September 2008; accepted March 2009